Journal of Volcanology and Geothermal Research 303 (2015) 7–15

Contents lists available at ScienceDirect

Journal of Volcanology and Geothermal Research

journal homepage: www.elsevier.com/locate/jvolgeores

He, Ar, N and C isotope compositions in Tatun Volcanic Group (TVG), Taiwan: Evidence for an important contribution of pelagic carbonates in the magmatic source

Emilie Roulleau [a,b,*], Yuji Sano [a,c], Naoto Takahata [a], Frank T. Yang [c], Hiroshi A. Takahashi [d]

[a] The University of Tokyo, Atmosphere and Ocean Research Institute, Kashiwa, Japan
[b] Andean Geothermal Centre of Excellence, Departamento de Geología, Universidad de Chile, Santiago, Chile
[c] National Taiwan University, Department of Geosciences, Taipei, Taiwan
[d] Geological Survey of Japan, AIST, Tsukuba, Japan

ARTICLE INFO

Article history:
Received 15 December 2014
Accepted 11 July 2015
Available online 22 July 2015

Keywords:
Tatun Volcanic Group
Ryukyu arc
Nitrogen
Helium
Carbon
Pelagic carbonate recycling

ABSTRACT

The Tatun Volcanic Group (TVG), Northeastern Taiwan, is considered to be the extension of the Ryukyu arc, and belongs to the post-collisional collapse Okinawa Trough. Strong hydrothermal activity is concentrated along the Chinshan fault, and Da-you-keng (DYK) represents the main fumarolic area where the most primitive isotopic and chemical composition is observed. In this study, we present chemical and He, Ar, C and N isotopic compositions of fumaroles, bubbling gas and water from hot springs sampled in 2012 and 2013. High $^3He/^4He$ ratios from DYK fumaroles (≈6.5 Ra) show a typical arc-like setting, whereas other sampling areas show a strong dependence of $^3He/^4He$ and $CH_4/^3He$ ratios with the distance from the main active hydrothermal area (DYK). This could mean strong crustal contamination and thermal decomposition of organic matter from local sediments. Carbon isotope compositions of DYK range from −6.67‰ to −5.85‰, and indicate that carbon contribution comes mainly from pelagic carbonates from the slab (limestone, mantle and sediment contributions are 63%, 19% and 18%, respectively). This is consistent with the negative $\delta^{15}N$ values (−1.4 ± 0.5‰) observed for DYK, implying a strong nitrogen-mantle contribution, and an absence of contribution from nitrogen-pelagic carbonates. These results have important consequences related to the Ryukyu subducted slab. In fact, the Ryukyu margin presents little in off scraping the sedimentary cover to the subducting plate that does not permit any nitrogen contribution in magma from TVG.

1. Introduction

The tectonic framework around Taiwan Island is very complex. Taiwan is located at the convergent boundary between the Eurasian and Philippine plates and marked by the collision of the Luzon volcanic arc with the Asiatic continental margin in the South (Fig. 1). Behind the Ryukyu trench, the spreading Okinawa trough has developed. The northern part of Taiwan is located at the western extrapolation of the Okinawa trough (Wang et al., 1999).

The Tatun Volcanic Group (TVG), in northeastern Taiwan is located in the area delimited by Chinshan and Kanchiao faults, strikes in the NE-SW direction (Fig. 1), and represents a large-scale Quaternary volcanic eruption. Since the last eruption occurred at 20 ka (Chen and Lin, 2002), the TVG is considered dormant. However, the high $^3He/^4He$ ratios (4.0–7.6 Ra, where Ra is the $^3He/^4He$ ratio of air) observed in the gas emissions from TVG, exhibit He mantle-derived characteristics, alluding to the actual existence of magmatic activity (Yang et al., 1999). Konstantinou et al. (2007) detected earthquake activity caused by hydrothermal circulation, and suggested that it is driven by the heat of degassing magma. Lee et al. (2008) repeatedly observed the fumarolic gases at TVG, and detected a co-seismic change in the $^3He/^4He$ ratio. Recently, a seismic tomography study from Wen et al. (2012) showed the existence of a tube-shaped, highly fractured ancient magma passage with high seismic velocities that parallel the Chinshan fault and a magma passage that extends to the southeast at a depth of about 20 km. This structure suggests a plutonic intrusion passage beneath TVG that may have been associated with the earlier subduction of the Philippine Sea plate. The melting of this subducted plate generated the magma intrusion that brought about the TVG geothermal activity. An important number of micro-earthquakes are located beneath the Chihsingshan volcano and DYK area. Most of these are volcano-tectonic earthquakes that are caused by a highly fractured crust, interpreted to be related to hydrothermal activities and their interaction between fluid-rock. All of the above studies support the existence of degassing magma beneath the TVG.

* Corresponding author at: Andean Geothermal Centre of Excellence (CEGA) Departamento de Geología, Universidad de Chile, Plaza Ercilla 803, Santiago, Chile. Tel.: +56 2 97871053.
E-mail address: eroulleau@ing.uchile.cl (E. Roulleau).

http://dx.doi.org/10.1016/j.jvolgeores.2015.07.017
0377-0273/

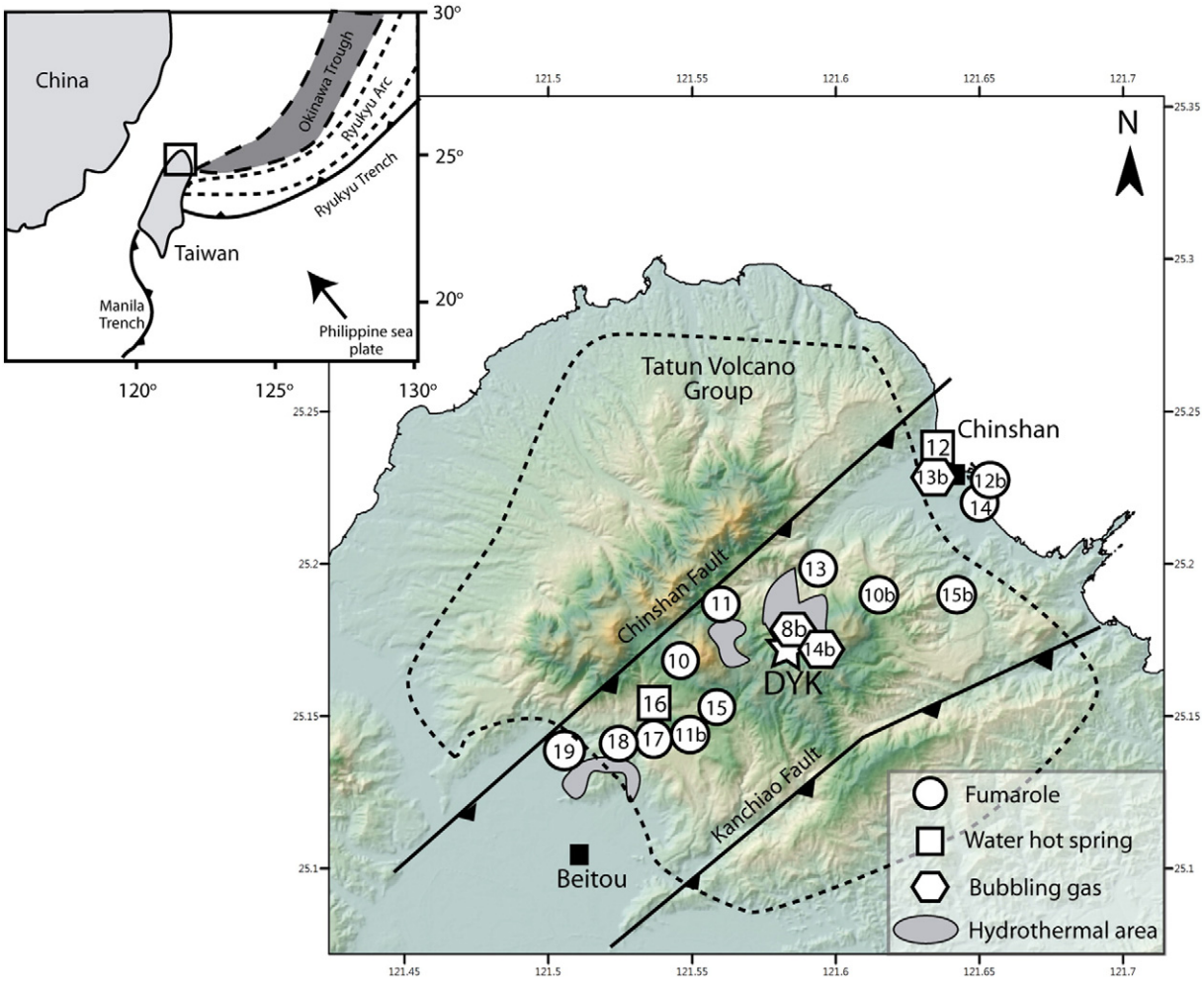

Fig. 1. Map of the geologic setting of Taiwan and location of sampling sites from the Tatun Volcanic Group (TVG).

Gas composition of TVG exhibits an affinity with convergent plate gases (Lee et al., 2008), suggesting that the degassing sources for the TVG gases were closely related to the subducting process of the Ryukyu arc. He isotopes from gas emissions demonstrated that more than 60% of helium is mantle-derived (Yang et al., 1999; Lee et al, 2008). Yang et al. (2005) reported a comparative study between the TVG and Kueishantao Islet (KST) gases. Kueisshantao Islet is an extrapolation of the extensive Okinawa trough, related to uprising of the mantle, and shows a high $^3He/^4He$ ratio (7.68 Ra) representing the large contribution from mantle He (MORB). Using the correlation between He and Sr isotopes, the authors showed that TVG is the result of MORB-subducted sediments mixing associated with probable crustal addition from local sediments. The $\delta^{13}C$–CO_2 values for TVG range from −3.28‰ to −7.02‰, revealing a variation in the sediment and limestone components, whereas the magmatic source is about constant (Yang et al., 2003; Lan et al., 2007). To explain these variations in C isotopic composition, the authors speculate on the opening of a gas path due to the extensional regime.

In this study, we investigated the gas composition and He, Ar, C and N isotopes in fumaroles, bubbling gases and hot springs from TVG in order to understand the origin of volatiles and to track processes leading to the observed signature.

2. Geology and geothermal manifestations at TVG

The TVG consists of about 20 volcanoes and volcanic domes covering an area of approximately 350 km^2, with the last eruption dated at 20 ka (Chen and Lin, 2002; Belousov et al., 2010; Chen et al., 2010). Eruption history of the TVG can be divided into two major periods. The first eruptive period began around 2.5–2.8 Ma, then ceased after about one million years. The second period started 1.5 Ma and continued until around 0.1–0.2 Ma (Song et al., 2000). Bedrock around the TVG is mostly hydrothermal-altered lower Miocene sedimentary rock and minor unaltered Wuchihshan Formation, composed of white sandstone and thin layers of shale and coal. Also present is the Mushan Formation which contains quartzite sandstone, gray-to-black shale and coal (Ho, 1988).

TVG is considered dormant because of its lack of previous historical eruptions. However, geothermal activities (hot springs and gas fumaroles) are well developed, suggesting that the TVG is still active. Major fumaroles and hot springs are distributed along the Chinshan reverse fault, indicating that the volcanic activity of TVG is related to the activity of this fault. The main thermal discharge is located at Da-You-Keng (DYK) and it presents the most vigorous fumarole emission with outlet temperature of 100 °C (Lee et al., 2008; Ohba et al., 2010). Other thermal discharges consist of boiling-bubbling and thermal water pools as well as small fumarole emissions with temperatures up to 100 °C (Lee et al., 2008; Ohba et al., 2010). Temperatures calculated through geothermometry are estimated at 189–210 °C (Ohba et al., 2010). The estimated CO_2/H_2O ratio for the magmatic component is comparable to that of some active volcanoes in Japan or other volcanic arcs, suggesting the enrichment of volatiles in the magmas beneath TVG (Ohba et al., 2010).

3. Samples and analytical methods

Two fumarole samples were collected from Da-You-Keng (DYK). Fumarolic gases were sampled using a titanium tube connected by a silicone tube to a lead glass bottle and cold trap. The lead glass bottle and

cold trap were plunged into a mixture of cold water and ice. Two water samples were collected from natural hot springs along with 12 bubbling gas samples (Table 1). Water from natural hot springs was sampled in lead glass containers using a manual pump. Bubbling gases were sampled using a lead glass container with vacuum valves at both ends, following a water displacement method. Dissolved gases from water samples were then extracted in the lab using a glass bottle under vacuum, which was plugged to the extraction line.

Nitrogen isotopic analyses were carried out at the Atmosphere and Ocean Research Institute (AORI), at the University of Tokyo, Japan. Measurements were done on a static magnetic-sector mass spectrometer VG3600, equipped with Faraday cups and calibrated against a purified atmospheric N standard. Details regarding the extraction procedures and general performance of the instruments are presented in Takahata et al. (1998). The nitrogen isotopic composition is given by the equation:

$$\delta^{15}N = \left(\left[{}^{15}N/{}^{14}N\right]_{sample}/\left[{}^{15}N/{}^{14}N\right]_{air} - 1\right) \times 1000. \quad (1)$$

The $\delta^{15}N$ values were corrected from blanks (Barry et al., 2012). The error in the $\delta^{15}N$ values reported in Table 1 is the propagated error in the isotopic measurement of N for the sample, the standard and the blank, assumed at 1σ. After nitrogen isotope measurements, the $^{28}N_2/^{40}Ar$ ratio was determined by measuring the $28^+/40^+$ ratio using the same mass spectrometer and calibrated against air standard, with an error assumed at 1σ.

The argon isotopic analyses were also performed at AORI. The $^{40}Ar/^{36}Ar$ ratios were measured using an online quadrupole mass spectrometer (Massmate100, ULVAC Co.) after purification using a hot Ti-getter. The error was 1–2% at 1σ.

The $^3He/^4He$ ratio was measured on a conventional noble gas mass spectrometer (Helix-SFT and VG-5400) at AORI. The $^4He/^{20}Ne$ ratio was measured using an online quadrupole mass spectrometer. Helium was separated from Ne using a cryogenic trap held at 40 °K (Sano and Wakita, 1988). The observed $^3He/^4He$ ratio was calibrated against atmospheric He. Experimental errors for $^4He/^{20}Ne$ and $^3He/^4He$ ratios are about 5% and 1% at 1σ with the Helix spectrometer and about 5% and 3.5% at 1σ with VG5400 spectrometer, respectively (Sano et al., 2008). The $^3He/^4He$ ratio is corrected for the presence of atmospheric He, using the $^4He/^{20}Ne$ ratio of the sample (Craig et al., 1978). It is assumed that ^{20}Ne in magmatic and crustal gases is negligible, and that essentially ^{20}Ne in geothermal gas samples is atmospheric. Accordingly:

$$Rc/Ra = \left(\left({}^3He/{}^4He\right)_{obs} - r\right)/(1-r) \quad (2)$$

$$r = \left({}^4He/{}^{20}Ne\right)_{ASW}/\left({}^4He/{}^{20}Ne\right)_{obs} \quad (3)$$

where Rc/Ra and $(^3He/^4He)_{obs}$ denote the air-corrected and observed $^3He/^4He$ ratios respectively. Variables $(^4He/^{20}Ne)_{ASW}$ and $(^4He/^{20}Ne)_{obs}$ are the ASW and observed $^4He/^{20}Ne$ ratios respectively. The total error of the corrected $^3He/^4He$ ratio is defined in Sano et al. (2006). The error assigned to the air-corrected $^3He/^4He$ ratio in Table 1 includes all possible $^3He/^4He$ errors.

The $\delta^{13}C$ values of CO_2 were measured by a continuous flow GC-IRMS system at the Geological Survey of Japan, National Institute of Advanced Industrial Science and Technology, Tsukuba. CO_2 was separated from the sample gas using a Carboxen GC capillary column at 50 °C with He carrier gas flowing at 4 mL/min. Three measurements were carried out for each sample, but only the average value is reported here. The δ-notation of the isotopic values is conventionally represented with respect to Vienna PeeDee belemnite (VPDB). Measurement errors of $\delta^{13}C$ are better than ±0.1‰.

The gas chemical compositions were determined by comparing peak heights of the sample with those of standard gases, using a quadrupole mass spectrometer at AORI. Experimental errors were estimated to be about ±10% by repeated measurements of standard samples. The measured blank for each component was negligibly small compared to the sample signal.

4. Results

Table 1 presents the chemical and the He, N, Ar and C isotopic compositions of hot springs, bubbling gases, and fumaroles from TVG.

4.1. Chemical compositions

The majority of fumarole, water-dissolved gas and bubbling gas samples had low O_2 content, inferior to 3%, except for three samples KS-12, DYK-8b and KS-13b that showed direct air contamination during sampling.

The N_2/Ar ratio in TVG ranged between 46 and 107, presenting the evidence of atmospheric component (the atmospheric and air-saturated water values were 84 and 38, respectively). However, two samples had an N_2/Ar ratio of 159 (DP-14) and 172 (SYK-10).

The $CO_2/^3He$ ratios were calculated from CO_2/He and $^3He/^4He$ ratios for each sample. The $CO_2/^3He$ ratios for water-dissolved gases and bubbling gases ranged between 26.19×10^9 (HS-16) and 0.99×10^9 (SHP-10b) whereas fumarolic gas, DYK-14b and DYK-8b, was 11.15×10^9 and 8.38×10^9, respectively. These $CO_2/^3He$ ratios for TVG were similar to those of average volcanic arc data (mean $CO_2/^3He = 1.5 \pm 1.1 \times 10^{10}$; Sano and Williams, 1996) and previous data (Yang et al., 2003; Fig. 2).

$CH_4/^3He$ ratios from TVG showed a high variation, ranging between 3.38×10^6 and 2.27×10^8.

4.2. He, N, Ar and C isotope compositions

The $^3He/^4He$ ratio normalized to the atmospheric ratio (Ra = 1.382×10^{-6}; Mabry et al., 2013) are presented with $^4He/^{20}Ne$ ratios in Fig. 3. Usually the $^3He/^4He$ Ra ratios are explained by the mixing between air-saturated water (ASW) or air component and the deep magmatic source with possible interaction from the crust. Samples showed two different mixing curves defined by $^3He/^4He$ ratios of 6.5 Ra and 4.8 Ra. Most of our samples had high $^4He/^{20}Ne$ (up to 140), consistent with magmatic fluids. Only KS-12 (0.339) had a high O_2 content which is indicative of direct air contamination.

Rc/Ra ratios covered the range of 4.53 Ra to 6.40 Ra (excluding KS-12). The high Rc/Ra was defined by DYK and Geng-Zi-Ping (GZP) samples that were from the most active areas. The average estimated from eight years of monitoring at DYK showed He magmatic source at 6.68 Ra (Lee et al., 2008), which was consistent with our $^3He/^4He$ data. The other localities also showed a concordance in $^3He/^4He$ between the two sampling campaigns (i.e. Dapu) and previous studies (Lan et al., 2007; Lee et al., 2008).

Finally, we point out that there was a particular variation of Rc/Ra with the distance from the main active area, DYK (Fig. 4A). Generally, high Rc/Ra ratios are close to DYK, and low Rc/Ra are located up to 10 km from DYK. There are some exceptions such as GZP and SHP suggesting that distance is not the only parameter that modifies the $^3He/^4He$ ratio in TVG. Ohba et al. (2010) reported He data of SHP, GZP and DYK from 2006. We note an important variation of He in SHP between Ohba's data (6.75 Ra), and our data (5.87 Ra). DYK (6.5–6.9 Ra) and GZP (4.65–6.47 Ra) data from Ohba et al. (2010) are slightly higher than our data but similar to Lee et al.'s (2008) data.

The $\delta^{15}N$ values for fumarole samples from DYK were −1.4 ± 0.5‰ and −1.2 ± 0.9‰ which was consistent with the MORB component (−5 ± 2‰; Sano et al., 2001). Water-dissolved gas and bubbling gas samples had a large range of $\delta^{15}N$, between +4.1 ± 0.7‰ and −1.5 ± 0.6‰.

The $^{40}Ar/^{36}Ar$ ratio of all samples ranged between 289.2 ± 8.7 and 324.9 ± 9.7 respectively. This is consistent with previous data on fumaroles and with other arc volcanoes (401 ± 278; Hilton et al., 2002).

Table 1
Isotopic and chemical composition of TVG fumarole, bubbling gas and water samples.

	Located	Sample	Date	Distance from DYK (km)	Latitude	Longitude	Temperature (°C)	pH	$^4He/^{20}Ne$	$^3He/^4He$ R/Ra	±	$^3He/^4He$ Rc/Ra	±	N_2/Ar	±	$\delta^{15}N$
SYK-10	Siao-You-Keng	Bubbling gas	2012	5.75	25°10′34″	121°32′50″	83	3.2	72.79	5.50	0.17	5.52	0.17	172	5	2.0
MT-11	Matsao	Bubbling gas	2012	3.75	25°10′39″	121°33′43″	82	–	50.48	4.57	0.14	4.59	0.14	83	3	1.7
KS-12	Jinshan	Water	2012	9	25°13′00″	121°38′33″	47	6.8	0.339	1.10	0.02	1.49	0.02	–	–	–
BY-13	Bayen	Bubbling gas	2012	3.25	25°11′38″	121°38′22″	66.6	2.5	72.19	4.68	0.05	4.70	0.05	107	3	1.5
DP-14	Dapu Spa Hotel	Bubbling gas	2012	9.16	25°12′59″	121°38′37″	35.5	1.8	140.64	4.88	0.15	4.89	0.15	159	5	2.4
CSL-15	Zhong Shan Lou	Bubbling gas	2012	4.5	25°09′12″	121°33′00″	37	4.85	50.54	5.20	0.16	5.23	0.16	101	3	3.1
HS-16	School Hushan	Water	2012	6.25	25°08′60″	121°32′10″	37.5	6.2	4.28	5.10	0.06	5.37	0.06	80	2	0.4
LFK-17	LFK	Bubbling gas	2012	6.75	25°08′40″	121°31′44″	25	4.6	44.84	5.24	0.16	5.26	0.16	89	3	4.1
LHK-18	Liou-Haung-ku	Bubbling gas	2012	8.25	25°08′40″	121°31′27″	31	3.23	39.35	5.34	0.16	5.37	0.16	80	2	4.0
TYK-19	Beitou	Bubbling gas	2012	10	25°08′19″	121°31′43″	52	1.38	3.94	4.44	0.13	4.70	0.13	46	1	1.9
DYK-8b	Da-You-Keng	Fumarole	2013	0	25°10′46″	121°34′48″	112.8	–	4.38	6.06	0.07	6.40	0.07	85	3	−1.4
SHP-10b	She-Huang-Ping	Bubbling gas	2013	3.25	25°10′56″	121°36′17″	35	–	39.15	5.87	0.06	5.90	0.06	73	2	0.0
LSK-11b	Leng-Shuei-Keng	Bubbling gas	2013	6	25°09′53″	121°33′45″	57	–	12.91	5.62	0.06	5.72	0.06	94	3	1.0
DP-12b	Dapu	Bubbling gas	2013	9.16	25°12′53″	121°38′40″	40	–	1.28	3.78	0.04	4.53	0.04	78	2	−1.5
KS-13b	Jinshan 2	Bubbling gas	2013	9	25°14′40″	121°37′50″	40	–	3.24	4.41	0.05	4.72	0.05	73	2	−1.4
DYK-14b	Da-You-Keng	Fumarole	2013	0	25°10′46″	121°34′48″	112.8	–	19.57	6.30	0.07	6.30	0.07	91	3	−1.2
GZP-15b	Geng-Zi-Ping	Bubbling gas	2013	5.5	25°11′11″	121°36′46″	60	–	35.57	6.31	0.07	6.36	0.07	99	3	0.5

Note: $CO_2/^3He$ and $CH4/^3He$ are calculated from CO_2/He and CH_4/He, and $^3He/^4He$ ratios. Error for $^4He/^{20}Ne$ is 5%.

The $\delta^{13}C$–CO_2 values for fumaroles from DYK were −5.85 ± 0.09‰ and −6.67 ± 0.39‰. while the values for hot springs and bubbling gases ranged from −4.66 ± 0.19‰ to −9.62 ± 0.08‰. The DYK $\delta^{13}C$–CO_2 values were similar to those proposed for MORB (−6.5 ± 2.2‰; Sano and Marty, 1995) and high temperature volcanic gases (−5.5 ± 2.2‰; Sano and Marty, 1995; Sano and Williams, 1996). There is no variation of $\delta^{13}C$–CO_2 values related to the type of sample, except for the unique water sample from Hushan School that was very low, suggesting an addition of CO_2 from local sediments. From Yang et al. (2003), the $\delta^{13}C$–CO_2 values for DYK (ca. −6.34‰) were similar to what we found in this study. For the other areas (SYK, LHK, MT, TIK, SHP and CSL), generally the $\delta^{13}C$–CO_2 values were higher (ca. −3.50‰) than our values.

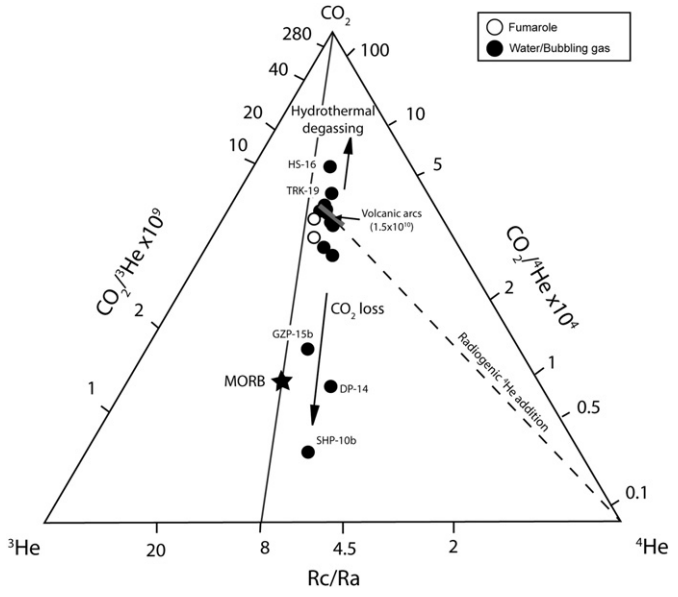

Fig. 2. Ternary diagram between ^3He, ^4He and CO_2 for fumarole, bubbling gases and water from TVG. For comparison, MORB (black star) and average volcanic arc (gray bar) fields are reported (Marty et al., 1989; Sano and Marty, 1995; Sano and Williams, 1996; Fourre et al., 2002; Hilton et al., 2002). The high $CO_2/^3He$ for HS-16 and TRK-19 are the result of hydrothermal degassing and preferential He loss. CO_2 addition can also play a rule for TRK-19 sample. The low $CO_2/^3He$ for GZP-15b, DP-14 and SHP-10b are the result of CO_2 loss by calcite precipitation. The dotted line represents the addition of radiogenic ^4He in the hydrothermal system. Symbols: Black circles are for bubbling gas and water samples. Empty circles are for DYK fumaroles.

Similar $\delta^{13}C$–CO_2 values were observed in Okinawa back-arc fluids (Ishibashi et al., 1995).

5. Discussion

The survey of geothermal fluids and gases from TVG shows that TVG is characterized by a large range of $^3He/^4He$, $\delta^{15}N$, $\delta^{13}C$–CO_2 and CO_2/He values. The results suggest that DYK has the most representative magmatic features similar to volcanic arc data (Sano and Marty, 1995; Sano et al., 2001; Hilton et al., 2002). In Fig. 2, 15 samples from this study are plotted on a CO_2–^3He–^4He ternary diagram (Giggenbach and Poreda, 1993a) to identify the general features of the He–CO_2 fluid characteristics of the TVG. Two component-mixing trajectories are plotted on this diagram. For reference we include (a) solid lines representing mixing between pure CO_2 and pure He (at a $^3He/^4He$ ratio of 8 ± 1 Ra: MORB) and (b) dotted lines representing mixing between radiogenic He and volcanic arc-like magmatic gas ($CO_2/^3He$: 1.5 ± 1.1 × 10^{10}; Sano and Williams, 1996). Most of our samples (fumaroles and bubbling gases) were consistent in He and CO_2 with the range of volcanic arc data

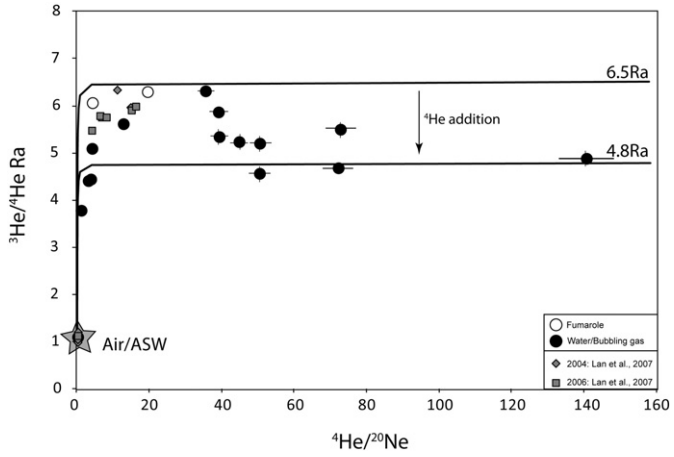

Fig. 3. $^3He/^4He$ Ra versus $^4He/^{20}Ne$ ratios for TVG samples. The magmatic source of $^3He/^4He$ range between 6.5 Ra and 4.8 Ra that is explained by ^4He addition from crust. The solubility of He and Ne for ASW are calculated using a temperature of 22 °C and a salinity of 0‰. The ASW-mantle curves are from a simple model of mixing. The error is equivalent to the size of the symbols if it is not observable.

±	$^{40}Ar/^{36}Ar$	±	$N_2/^{36}Ar$	±	$\delta^{13}C–CO_2$ (‰)	±	$CO_2/^3He * 10^{-9}$	$CH_4/^3He * 10^{-8}$	He * 10^{-5} ccSTP/g 22 °C	N_2/He	He/Ar	O_2 (%)	CH_4 (%)	N_2 (%)	Ar (%)	H_2S (%)	CO_2 (%)
0.7	308.2	9.3	52,906	2255	−5.54	0.14	12.41	2.11	1.22	7922	0.015	1.42	1.49	7.26	0.06	2.38	87.55
0.7	317.8	9.5	34,885	1478	−5.05	0.01	8.02	1.64	1.21	1429	0.112	0.02	1.93	2.58	0.02	0.71	94.75
–	–	–	–	–	−5.16	0.01	11.29	2.24	0.84	2137	0.051	0	1.89	2.81	0.03	0.34	95.03
0.7	–	–	–	–	–	–	–	–	0.006	–	–	22.58	0.01	73.77	1.04	0.00	2.60
0.7	324.9	9.7	52,768	2243	−4.66	0.19	2.80	1.40	2.36	1651	0.134	0.06	4.39	7.58	0.0.3	0.00	87.93
0.8	316.5	9.5	32,364	1367	−5.68	0.06	12.93	0.37	0.84	2955	0.045	0	0.26	2.81	0.02	7.66	89.49
0.8	–	–	–	–	−9.62	0.08	26.19	0.04	0.071	19,319	0.004	0.49	0.01	9.31	0.13	0.00	90.06
0.7	295.4	8.9	24,876	1060	−5.46	0.04	11.96	1.15	0.75	3539	0.030	0	0.91	3.82	0.04	0.50	94.79
0.8	–	–	–	–	−5.31	0.06	8.83	1.03	0.66	2878	0.037	0	1.10	4.12	0.04	0.32	94.56
0.8	–	–	–	–	−6.64	0.09	20.62	2.27	0.066	21,022	0.003	0	0.93	13.84	0.23	0.70	84.50
0.5	289.2	8.7	24,518	1040	−5.85	0.09	8.36	0.04	–	16,826	0.006	4.05	0.04	18.30	0.19	0.05	77.38
0.6	298.3	8.9	21,891	929	−6.99	0.03	0.99	0.28	0.65	9130	0.009	0.31	1.28	51.60	0.60	0.00	46.20
0.6	302.0	9.1	28,366	1203	−6.23	0.01	13.56	0.57	0.22	3072	0.040	0.14	0.40	2.75	0.02	1.06	95.47
0.6	300.1	9.0	23,496	987	–	–	–	–	0.021	–	–	–	–	–	–	–	–
0.6	298.2	8.9	21,711	921	−5.25	0.04	12.36	2.22	0.054	24,651	0.003	2.22	1.26	22.73	0.27	0.00	70.41
0.9	300.3	9.0	27,280	1157	−6.67	0.39	11.15	0.05	–	7266	0.015	0.05	0.04	6.79	0.06	0.10	91.96
0.9	305.5	9.2	30,275	1284	−6.20	0.04	3.21	0.24	0.59	3394	0.036	0.24	0.66	10.47	0.09	0.22	87.67

(1.5×10^{10}; Sano and Williams, 1996). DYK fumaroles had one of the highest Rc/Ra (6.30 Ra and 6.40 Ra), and their $CO_2/^3He$ (1.12×10^{10} and 8.38×10^9) were consistent with volcanic arcs worldwide (Sano and Williams, 1996). This observation is the first implication that the He and CO_2 TVG magmatic source is derived from mantle wedge and subducted components. The other localities show some variable He, CO_2 and N_2 characteristics that we will define in the following section before defining the magmatic features of TVG.

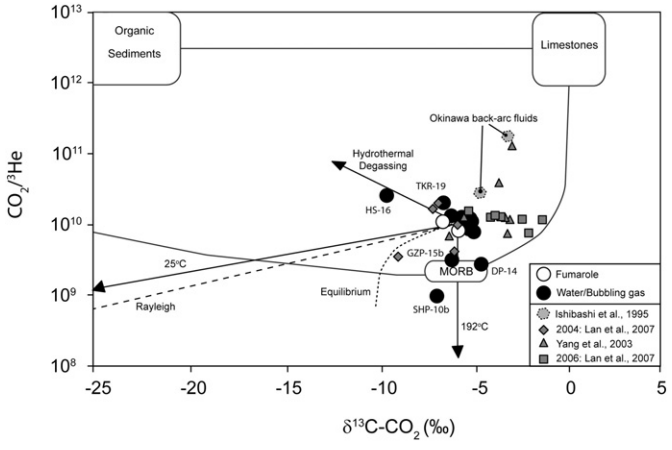

Fig. 4. $CO_2/^3He$ versus $\delta^{13}C–CO_2$ for TVG samples compared to MORB, organic sediments and marine limestone. The solid lines represent mantle-organic sediments, mantle-marine limestone, and organic sediments-marine limestone binary mixing lines. MORB has $\delta^{13}C–CO_2 = -6.5 \pm 2.2$‰ and $CO_2/^3He = 2 \times 10^9$ (Marty et al., 1989; Sano and Marty, 1995; Sano and Williams, 1996). $\delta^{13}C–CO_2$ and $CO_2/^3He$ values for organic sediments are -30 ± 10‰ and 1×10^{13} (Sano and Marty, 1995; Hoefs, 2009) and 0 ± 2‰ and 1×10^{13} for marine limestone (Sano and Marty, 1995; Hoefs, 2009). Symbols: Black circles are for bubbling gas and water samples. Empty circles are for DYK fumaroles. Previous data from TVG (Yang et al., 2003; Lan et al., 2007) and Okinawa back-arc (Ishibashi et al., 1995) fluids are reported. Dark lines represent trajectories for CO_2 loss by calcite precipitation at a temperature of 25 °C (fractionation factor = −10‰) and 192 °C (fractionation factor = 0‰). The starting point is DYK. Our three samples (GZP-15, DP-14 and SHP-10b) fall on the fractionation line at 192 °C. The samples (HS-16 and TRK-19) with high $CO_2/^3He$ ratios and low $\delta^{13}C–CO_2$ are the result of hydrothermal degassing. Rayleigh distillation and batch equilibrium curves starting from DYK samples are presented. See text for fractionation factor (Javoy et al., 1978; Ray et al., 2009).

5.1. Hydrothermal degassing

Within a hydrothermal system, gas separation has the potential to fractionate both the gas ratio ($CO_2/^3He$) and the $\delta^{13}C$-CO_2 value (Giggenbach and Poreda, 1993b; Ray et al., 2009). The observed $CO_2/^3He$ ratios in gas and water are different and consistent with gas separation. Helium is preferentially partitioned in the gas phase, whereas the more soluble CO_2 is concentrated in aqueous liquid. This physical process induces an increase of $CO_2/^3He$ in residual water and can induce an isotopic fractionation of $^{13}C/^{12}C$ ratios (lower $\delta^{13}C$-CO_2 values; Vogel et al., 1970).

As shown in Fig. 2, two samples (HS-16 and TRK-19) had high $CO_2/^3He$ (26.19×10^9 and 20.62×10^9) compared to DYK fumaroles, suggesting He loss or CO_2 addition from local sediments. These samples also had low $\delta^{13}C–CO_2$ values (mainly HS-16; −9.62‰ and TRK: −6.64‰; Fig. 4) compared to arc fumarolic gases (Sano and Marty, 1995). HS-16 water sample had a Rc/Ra (5.37 Ra) similar to other bubbling gas samples suggesting no crustal contamination. TRK-19 showed a low Rc/Ra ratio (4.70 Ra), probably due to crustal contamination.

Fig. 5 shows the He contents for each hot spring and bubbling gas sample, estimated using $^4He/^{20}Ne$ and ^{20}Ne content (1.65×10^{-7}ccSTP/g) at 22 °C (estimated that ^{20}Ne content is

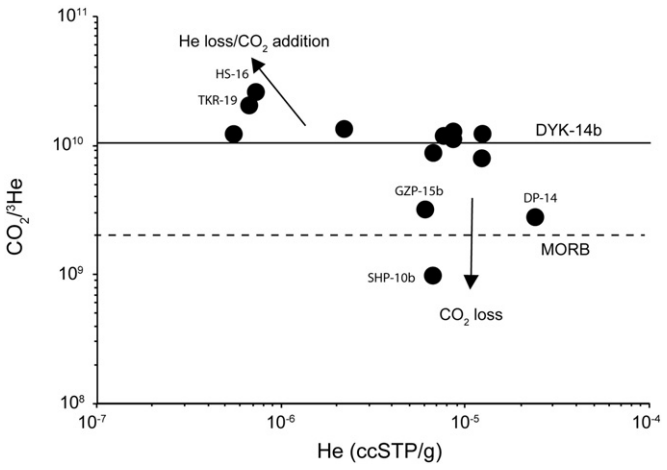

Fig. 5. $CO_2/^3He$ versus He concentration for bubbling gas and water. We observed that some samples show He loss or CO_2 addition, and others show CO_2 loss.

constant in the system). He contents for hot spring and bubbling gas samples are plotted with $CO_2/^3He$ ratios. $CO_2/^3He$ ratios from DYK-14b are reported as a reference of magmatic source. Most bubbling gas samples are plotted along the DYK reference line indicating that these samples were not affected by physical processes and represent a real magmatic signature. HS-16 (water) had lower He content associated with the highest $CO_2/^3He$ ratios indicating a vapor-liquid partitioning and the preferential loss of He. TKR-19 could be more related to the addition of CO_2 from local sediments such as sandstone, increasing the $CO_2/^3He$ ratio and decreasing the $^3He/^4He$ ratio.

5.2. Magmatic degassing vs. preferential CO_2 loss by calcite precipitation

Samples unaffected by gas phase partitioning were evaluated for other He–CO_2 controls. Fig. 2 shows three bubbling gas samples (GZP-15b, SHP-10b and DP-14) had low $CO_2/^3He$ ratios compared to volcanic arc data and DYK fumarole samples. This suggests a CO_2 loss from the magmatic/hydrothermal system (Giggenbach and Poreda, 1993a,b). For DP-14, the low $CO_2/^3He$ was associated with a slightly higher $\delta^{13}C$ value than DYK samples (Fig. 4). For GZP-15b and SHP-10b, the $\delta^{13}C$ value was slightly lower, but not significantly different from other samples (Fig. 4). Two processes possibly explain a low $CO_2/^3He$ observed in three samples from TVG: (1) magma degassing and (2) CO_2 loss by calcite precipitation.

5.2.1. Magmatic degassing

Degassing of andesitic-basaltic magma can produce a low $CO_2/^3He$ in residual melt as well as the $\delta^{13}C$ values (Javoy et al., 1978; Hilton et al., 1998). For the He–CO_2 elemental fractionation, the fractionation factor (α) is defined as $(CO_2/^3He)_{vap}/(CO_2/^3He)_{melt}$ as the inverse ratio of the solubility of He and CO_2 in parental melt. For a melt of tholeiitic composition, α is ~2.35 (Hilton et al., 1998). In this way, preferential loss of CO_2 occurs during melt degassing, and causes a decrease in the $CO_2/^3He$ ratio for the gas remaining in the melt. Loss of CO_2 from the melt will simultaneously decrease the $\delta^{13}C$ of the residual CO_2 (isotopic fractionation factor proposed is −4‰ corresponding to α: 0.996; Javoy et al., 1978). Two models of degassing can be expected: batch equilibrium (closed system) and Rayleigh distillation (open system). For these two processes of degassing, we assume an initial $CO_2/^3He$ of 9.76×10^9 and a $\delta^{13}C$ value of −6.26‰ (average of $CO_2/^3He$ and $\delta^{13}C$ from DYK fumaroles).

Using the Rayleigh distillation equation, $CO_2/^3He_{residual} = CO_2 / {}^3He_{initial} \times F^{(\alpha - 1)/\alpha}$, to get the lower $CO_2/^3He$ ratios (6.9×10^8) the system lost 98.9% of its CO_2; whereas the corresponding $\delta^{13}C$ values (calculated using the relationship: $\delta^{13}C_{residual} = \delta^{13}C_{initial} - 1000 \times F \exp(\alpha - 1) - 1$; Javoy et al., 1978) was −24.9‰. It is notable that TVG samples were below the Rayleigh distillation degassing curve (Fig. 4), suggesting that this process does not occur and does not explain the low $CO_2/^3He$ ratios observed in TVG.

Similarly, in the case of batch equilibrium degassing (using $\delta^{13}C_{residual} = \delta^{13}C_{initial} + (1 - F) \times 1000 \ln(\alpha)$ and $CO_2/^3He_{residual} = CO_2/^3He_{initial} \times F^{\wedge}((\alpha - 1)/\alpha$, Javoy et al., 1978; Ray et al., 2009), the degassing curve did not fit the TVG data. With this mode of degassing, the minimum possible for $CO_2/^3He$ and $\delta^{13}C$ is 6.9×10^8 and −10.2‰, respectively (Fig. 4).

Thus, in both batch equilibrium and Rayleigh degassing models, the calculated $\delta^{13}C$ value is too low compared to what we observed in TVG samples.

5.2.2. Preferential CO_2 loss by calcite precipitation

Another possibility to explain low $CO_2/^3He$ is CO_2 loss by calcite precipitation. CO_2 loss by calcite precipitation can occur during the cooling/mixing history of the hydrothermal system and produces a low $CO_2/^3He$ ratio (Hilton et al., 1998). Fractionation between $CaCO_3$ and CO_2 gas can be calculated theoretically. Temperature dependence for C soluble species with respect to $CaCO_3$ is well known (Bottinga, 1969). At temperatures less than 192 °C, calcite is enriched in ^{13}C relative to residual CO_2, thus the fractionation factors are −3‰ at 100 °C and −10‰ at 25 °C. However, at temperatures greater than 192 °C, calcite is depleted in ^{13}C relative to residual CO_2 and the fractionation factor is around 0‰ (Sano and Marty, 1995; Ray et al., 2009).

Fig. 4 shows $CO_2/^3He$ vs. $\delta^{13}C$-CO_2 values to illustrate the effect of calcite precipitation at two different temperatures, 25 °C and 192 °C. Calcite precipitation at 25 °C enables $CO_2/^3He$ and $\delta^{13}C$-CO_2 values in CO_2 residual gas to decrease, but it does not explain our data. Alternatively, calcite precipitation at 192 °C has the capacity to decrease $CO_2/^3He$ ratios without any modification of $\delta^{13}C$-CO_2 values. However, our samples do not fit this curve. Thus, for GZP-15b and SHP-10b sample values (which show a decrease in $CO_2/^3He$ and $\delta^{13}C$-CO_2), we suggest that these two samples can be explained by the precipitation of calcite at temperatures between 25 °C and 192 °C.

As previously mentioned, calcite precipitation at temperatures greater than 192 °C produces a positive fractionation factor inducing a higher $\delta^{13}C$-CO_2 value in CO_2 residual gas. Calcite precipitation can also explain the sample DP-14, which shows low $CO_2/^3He$ and high $\delta^{13}C$-(CO_2) compared to DYK fumarole samples. We can also note that sample DP-14 can be affected by crustal contamination, which could explain the higher $\delta^{13}C$-CO_2 value. This sample also had a Rc/Ra ratio lower (4.89 Ra) than DYK samples (~6.35 Ra), which can be an argument for crustal addition.

5.3. Crustal contamination: He, N and CH_4 characters

Crustal contamination has the potential to contribute to the isotopic variations observed in TVG. $^3He/^4He$, $CO_2/^3He$ ratios, $\delta^{15}N$ and $\delta^{13}C$–CO_2 values are known to be influenced by the gradual addition of radiogenic ^4He, N_2 and CO_2 from crustal rocks (Sano et al., 1998).

Fig. 6 illustrates the crustal involvement in TVG fluids for He. The $CO_2/^3He$ ratios and $\delta^{13}C$–CO_2 are not reported because they do not show any correlation with distance due to CO_2 fractionation; and the $\delta^{15}N$ values show unclear correlation. The distance is calculated from the main active area, DYK. He isotopes clearly show a negative correlation. Fig. 7A shows a negative correlation between Rc/Ra and $CH_4/^3He$ ratios indicative of an addition of ^4He and CH_4 coming from the same source. The high $CH_4/^3He$ ratio observed in the magmatic-hydrothermal system suggests the presence of thermogenic methane ($CH_4/^3He$: 10^8–10^{11}) associated with the thermal decomposition of organic matter from local sediments such as sandstone (Chen and Wu, 1971; Snyder et al., 2003).

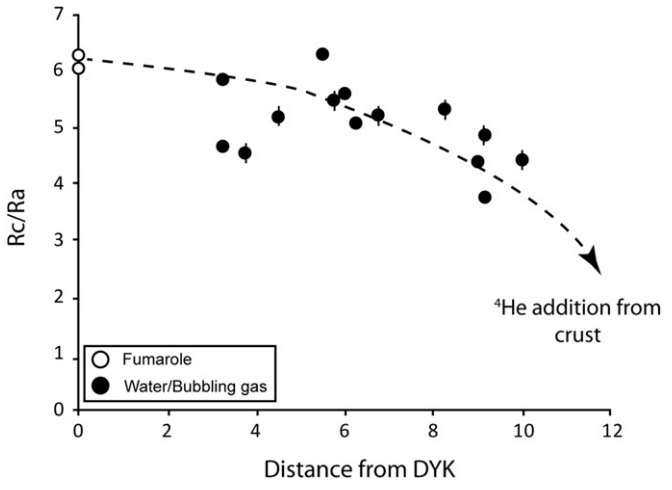

Fig. 6. Rc/Ra versus distance from DYK. Decreasing $^3He/^4He$ Ra indicates crustal contamination by host sediments. Symbols: Black circles are for bubbling gas and water samples. Empty circles are for DYK fumaroles. The error is equivalent to the size of the symbols if it is not observable.

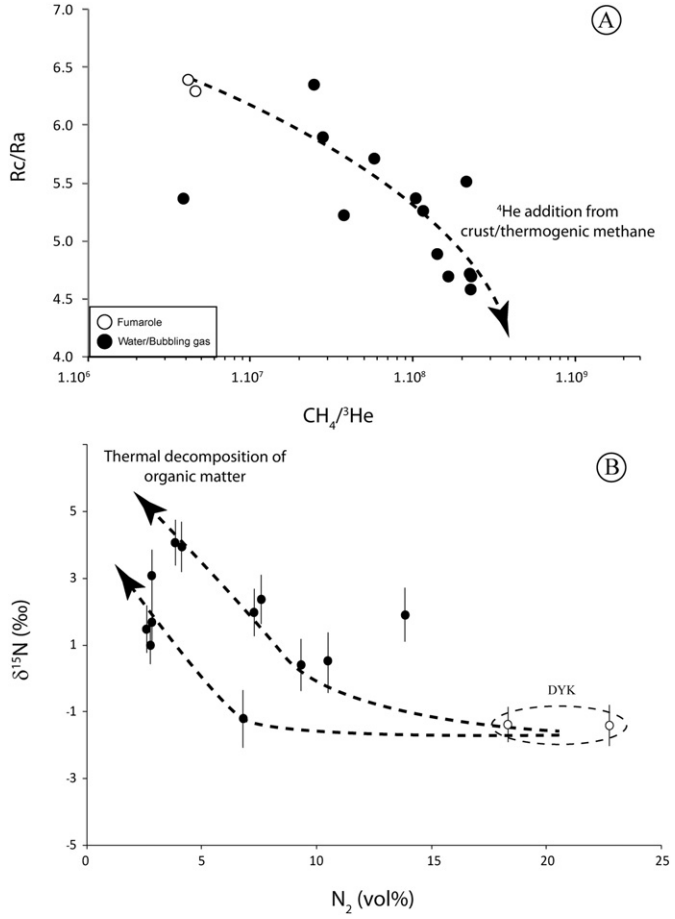

Fig. 7. A) Negative correlation between Rc/Ra and $CH_4/^3He$ related to crustal contamination by local sediments (^4He addition) and thermal decomposition of organic matter producing thermogenic methane (Snyder et al., 2003). B) $\delta^{15}N$ versus N_2 contents (vol%). The negative correlation is due to the fractionation exchange between N_2 and NH_4^+ related to the thermal decomposition of organic matter from local sediments. This process induces an increase of $\delta^{15}N$ values and a decrease of N_2 contents, and leads to the formation of $NH4^+$.

High $CH_4/^3He$ values from TVG are also associated with high $\delta^{15}N$ values (up to +4.1‰). An enrichment of ^{15}N, by thermal decomposition of organic matter from the crust, leads to the formation of $NH4^+$ (Sadofsky and Bebout, 2000). Haendel et al. (1986) calculated a fractionation factor for isotopic exchanges between N species ($N_2\backslash NH_4^+\backslash NH_3^+$) contained in rocks and metamorphic/hydrothermal fluids. The authors showed that $\delta^{15}N$ increased and the N content decreased with the increase of the metamorphic grade temperature. Chen and Sung (2009), studied the chemistry of Taiwanese hot springs and observed a high amount of $NH4^+$ (1.1 to 5.46 mg/L^{-1}) in the TVG hot springs. In Fig. 7B, a negative correlation between $\delta^{15}N$ values and N_2 contents was observed in TVG samples. These results suggest a thermal decomposition from organic matter from local sediments (sandstone; Chen and Wu, 1971) producing $NH4^+$ and the increase of $\delta^{15}N_2$ values.

Yang et al. (2003) reported nitrogen isotope data for two localities, CSL and LHK. The $\delta^{15}N$ values are +0.78‰ and around +0.67‰ respectively. However, in this study, we found the same values to be 3.1‰ and +4‰ respectively. Furthermore, there was a large variation of $\delta^{15}N$ values, +2.4‰ (DP-14) and −1.5‰ (DP-12b), between the two sampling campaigns for the Dapu area. Because there are no variations in He isotopes, these variations could be the result of the appearance or increasing of isotopic fractionation for exchanges between N species ($N_2\backslash NH_4^+\backslash NH_3^+$) related to thermal decomposition of organic matter.

5.4. Deep magmatic source for Tatun Volcanic Group

As discussed in the previous sections, our samples were affected by different physical processes that modified the initial isotopic composition. The most primitive magmatic source was defined by DYK fumaroles and GZP bubbling gases.

5.4.1. Helium isotopes

Helium isotope compositions in subduction zones ranged from 5 Ra to 8 Ra (Marty et al., 1989; Poreda and Craig, 1989; Sano and Marty, 1995; Sano and Williams, 1996; Fourre et al., 2002). Based on the correlation between $^3He/^4He$ versus $^4He/^{20}Ne$ (Fig. 3), the He isotopic magmatic source for TVG as defined by DYK fumaroles and GZP bubbling gas was 6.5 Ra. This result is consistent with the previous studies on the DYK area that showed the average $^3He/^4He$ ratio to be 6.68 Ra (Yang, 2000; Yang et al., 2003; Lee et al., 2008; Ohba et al., 2010). Yang et al. (2005) reported a comparative study between the TVG and Kueishantao Islet (KST) gases. Kueisshantao Islet is an extrapolation of the extensive Okinawa trough, related to uprising of the mantle, and shows a high $^3He/^4He$ ratio (7.68 Ra) representing the large contribution from mantle He (MORB). Thus, the primordial source of $^3He/^4He$ from DYK (and TVG in general) represents the MORB-subducted sediments mixing associated with probable crustal addition from local sediments.

5.4.2. Nitrogen isotopes

To better constrain the signature of the deep source, and determine the proportions of all components involved in our analysis, we present a plot of $\delta^{15}N$ versus $N_2/^{36}Ar$ (Fig. 8) where the nitrogen compositions of TVG indicate a mixing between three components (Sano et al., 2001): ASW (0‰; 1.8×10^4), crust (+7 ± 4‰; 6×10^6), and mantle (-5‰; 6×10^6). The mixing curve equations are as follows:

$$\delta^{15}N_{obs} = A\ \delta^{15}N_{ASW} + M\ \delta^{15}N_{Mantle} + S\ \delta^{15}N_{Sed} \quad (4)$$

$$1/\left(N_2/^{36}Ar\right)_{obs} = A/\left(N_2/^{36}Ar_{ASW}\right) + M/\left(N_2/^{36}Ar_{Mantle}\right) + S/\left(N_2/^{36}Ar_{Sed}\right) \quad (5)$$

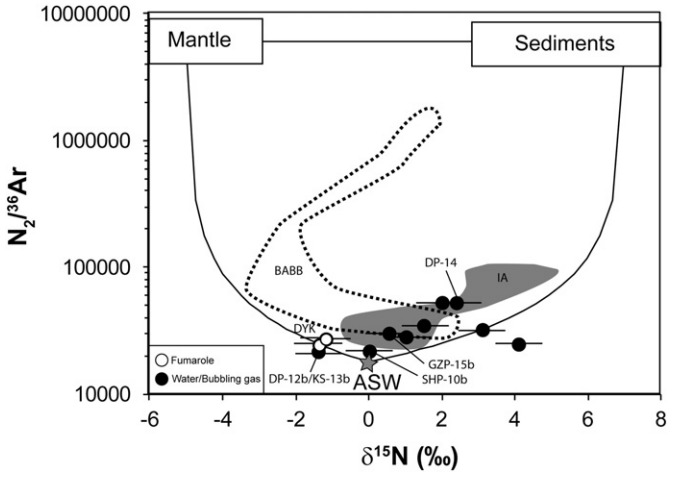

Fig. 8. $N_2/^{36}Ar$ versus $\delta^{15}N$ for TVG samples, as well as for the sediments, mantle, and ASW (Sano et al., 2001). Solid lines represent mantle-sediments, mantle-ASW, and sediments-ASW binary mixing lines, where starting compositions are ASW (0‰; 1.8×10^4), crust (+7 ± 4‰; 6×10^6), and mantle (-5‰; 6×10^6) from Sano et al. (2001). Back-arc basin basalt (BABB) and island arc (IA) domains are reported from Sano et al. (2001). The positive correlation of our samples shows the mixing between ASW and sediments from host rocks representing crustal contamination. Samples from DYK, DP-12b and KS-13b show a negative $\delta^{15}N$ and low $N_2/^{36}Ar$ explain the mantle contribution. Symbols: Black circles are for bubbling gas and water samples. Empty circles are for DYK fumaroles. The error is equivalent to the size of the symbols if not observable.

$$M + S + A = 1 \quad (6)$$

where obs, ASW, Mantle, and Sed refer to: observed value, ASW, mantle, and sediments respectively. A, M, and S are the mass of air, mantle, and sediments respectively. The results of these calculations are presented in Table 2.

Most of our samples from bubbling gases (including GZP-15) and water hot springs showed moderate to high $\delta^{15}N$ values (+0.5‰ to +4.1‰) and high $N_2/^{36}Ar$ ratios (30,275 to 52,906), demonstrating a sizeable proportion of air (up to 62%) and sediment (up to 47.5%) components, compared to the mantle component (21.5%). High sediment contribution is clearly the result of thermal decomposition of organic matter from local sediments (increasing of $\delta^{15}N$ values), as shown in Fig. 7b. On the other hand, four samples from fumaroles (DYK samples) and bubbling gases (DP-12b and KS-13b) showed negative $\delta^{15}N$ values (−1.4‰ to −1.2‰) and low $N_2/^{36}Ar$ ratios (21,711 to 27,280), resulting in a significant proportion of air (up to 71%) and mantle (up to 29%) components and a minor sediment (2.5%–0.5%) component. In subduction zones, nitrogen is usually recycled from subducted sediments (Sano et al., 2001) based on positive $\delta^{15}N$ values (Fig. 8; IA domain). In the case of TVG, it appears as though nitrogen derived subducted sediments are minor or almost nonexistent. This suggests that nitrogen mainly comes from mantle components, as observed in Costa Rica (Fischer et al., 2002) and in back-arc fluids (BABB; Fig. 8). In Costa Rica, the negative $\delta^{15}N$ values (−3‰) are the result of the absence of pelagic subducted sediments in the Costa Rica trench. This explanation is supported by the low ^{10}Be observed in this area (Morris et al., 1990), and by the presence of pelagic carbonates in the slab. In the case of the Ruykyu arc, the oceanic convergent margin is extremely rapid, which causes little trench sediment related to the short time available to deposit the trench section. Thus, the margin shows little impact in off scraping the sedimentary cover to the subducting plate (Clift and Vannucchi, 2004). On the other hand, Ryukyu limestone is observed in the Ryukyu arc at the northern corner of Taiwan (Ujiie and Ujiie, 1999). Bebout (1996) noted that the N concentration in oceanic pelagic sediments can vary from 70 to 600 ppm; however, pelagic limestone (100% calcite) may contain essentially no N. The negative $\delta^{15}N$ values observed in TVG are the result of the small amount of pelagic sediment subducted in the margin as well as the absence of contribution from nitrogen-pelagic carbonates; but we cannot exclude the possible involvement from Okinawa back-arc fluid.

Dapu (DP-12b) and Jinshan (KS-13b) samples are far from the DYK area (9 km) but they showed negative $\delta^{15}N$ values (−2.1‰ and −1.6‰). These two active hydrothermal areas appear to be related exclusively to the Chinshan fault.

5.4.3. Carbon isotopes

The $\delta^{13}C$–CO_2 and $CO_2/^3He$ ratios have been monitored since 1999 by Lan et al. (2007) and Yang et al. (2003, 1999). The $\delta^{13}C$–CO_2 from fumaroles and soil gases show a wide range of compositions, from −2.17‰ to −9.02‰ (Lan et al., 2007). Between 2004 and 2006 (soil gas campaigns), the $\delta^{13}C$–CO_2 values varied from an average of −7.02‰ to −3.31‰ respectively. The authors explained this range of $\delta^{13}C$–CO_2 values by the opening of gas paths in this area, since northern Taiwan is in an extensive tectonic setting. The $\delta^{13}C$–CO_2 value reported from DYK fumaroles is −6.34‰ (Yang et al., 2003) similar to our $\delta^{13}C$–CO_2 value (−6.67‰, DYK-14b). Our $\delta^{13}C$–CO_2 values ranged between −6.67‰ and −5.05‰ (excluding samples modified by physical processes). The average was −5.67‰, and represents an intermediate $\delta^{13}C$–CO_2 value compared to the 2004 and 2006 samples.

One approach for assessing the carbon origin in subduction zones is the three-component mixing model proposed by Sano and Marty (1995). Based on their $CO_2/^3He$ and $\delta^{13}C$–CO_2 characteristics, samples are described by a carbon mixture made of marine carbonates and mantle and organic sediments. $\delta^{13}C$–CO_2 of the MORB component is −6.5 ± 2.5‰ (Sano and Marty, 1995; Sano and Williams, 1996). In contrast, $\delta^{13}C$–CO_2 of sediments varies between two major components (Hoefs, 2009): organic sediments (−40‰ to −20‰), and marine sediments (0 ± 2‰). Fumarolic gases in subduction zones have $\delta^{13}C$–CO_2 of −5.5 ± 2.2‰ (Sano and Marty, 1995; Sano and Williams, 1996; Snyder et al., 2001). The mixing curve equations are as follows:

$$\delta^{13}C{-}CO_{2obs} = L\ \delta^{13}C_{Lim} + M\ \delta^{13}C_{Mantle} + S\ \delta^{13}C_{Sed} \quad (7)$$

$$1/\left(CO_2/^3He\right)_{obs} = L/\left(CO_2/^3He_{Lim}\right) + M/\left(CO_2/^3He_{Mantle}\right) + S/\left(CO_2/^3He_{Sed}\right) \quad (8)$$

$$L + M + S = 1 \quad (9)$$

where obs, Lim, Mantle, and Sed refer to: observed value, limestone, mantle, and sediments respectively; L, M, and S are the mass of limestone, mantle, and sediments respectively. The results of calculations are presented in Table 3.

The estimated proportions of carbon from DYK are 19% mantle, 63% limestone (pelagic carbonates) and 18% sediment components, suggesting that carbon comes mainly from the pelagic carbonates (Table 3). This result is consistent with nitrogen origin contribution proposed in the previous section.

The possible variation of carbon composition over time could be the result of the variable amount of sediment and limestone incorporated in the subducted zone and the variation of crustal contamination from local sediments. The $\delta^{13}C$–CO_2 values from Okinawa back-arc fluids (Fig. 4) ranged between −5‰ and −3.8‰ (Ishibashi et al., 1995), meaning that the variation observed in carbon composition of TVG may be influence from the extensional Okinawa trough.

Table 2
Nitrogen composition model for TVG samples.

	Nitrogen contribution		
	Air	Mantle	Sediment
SYK-10	34.00%	21.50%	44.50%
BY-13	53.00%	15.00%	32.00%
DP-14	34.00%	18.50%	47.50%
CSL-15	55.00%	0.50%	44.50%
LFK-17	–	–	–
DYK-8b	70.00%	29.00%	1.00%
DYK-14b	70.00%	27.50%	2.50%
GZP-15b	59.00%	20.00%	21.00%
LSK-11b	62.00%	14.00%	24.00%
KS-13b	71.00%	28.25%	0.75%
DP-12b	71.00%	28.50%	0.50%

Table 3
Carbon composition model for TVG samples. Samples affected by physical processes are excluded.

	Carbon contribution		
	Limestones	Mantle	Organic Sed.
SYK-10	69.00%	16.00%	15.00%
Mt-11	68.50%	18.00%	13.50%
BY-11	63.50%	25.00%	11.50%
CSL -15	68.90%	15.50%	15.60%
LFK-17	68.70%	17.30%	14.50%
LHK-18	64.00%	23.50%	12.50%
DYK-8b	62.50%	23.00%	14.50%
LSK-11b	67.50%	15.00%	17.50%
KS-13b	70.00%	16.00%	14.00%
DYK-14b	63.00%	19.00%	18.00%

6. Concluding remarks

Fumarolic gases of DYK showed the most primitive composition in He, N and C isotopes. For the other samples, He and N isotopic compositions and $CH_4/^3He$ ratios were clearly controlled by the thermal degradation of organic matter and crustal contamination from local sediments. The $CO_2/^3He$ ratios and $\delta^{13}C–CO_2$ values showed large variations related to physical processes which affect water and bubbling gas samples as hydrothermal degassing and calcite precipitation. He magmatic source was estimated at 6.5 Ra, but showed variation depending on new pulses of gas from the opening of a local fracture. DYK, DP and KS areas showed negative $\delta^{15}N$ values (around −1.4‰) comparable to MORB data. It appears that nitrogen-derived subducted sediments are minor or almost nonexistent, suggesting that nitrogen comes mainly from the mantle component. These results have important consequences related to the Ryukyu subducted slab, indicating that the Ryukyu margin shows little in off scraping the sedimentary cover to the subducting plate. Limestones observed in the Ryukyu arc indicate the absence of contribution of nitrogen-pelagic carbonates. This argument is supported by the substantial limestone contribution observed with $\delta^{13}C–CO_2$ values (63%).

Acknowledgments

We thank the anonymous reviewers and the editor Alessandro Aiuppa for their thoughtful reviews. We wish to thank Pr. Yang's team, particularly E. Chen and L. Wen, for their help during fieldwork. E. Roulleau's research was funded through JSPS grant no. P11713 and CONICYT/FONDECYT no. 11130351. This paper is dedicated to Pr. Yang who passed away much too early.

References

Barry, P.H., Hilton, D.R., Halldórsson, S.A., Hahm, D., Marti, K., 2012. High precision nitrogen isotope measurements in oceanic basalts using a static triple collection noble gas mass spectrometer. Geochem. Geophys. Geosyst. 13 (Q01019).
Bebout, G.E., 1996. Volatile transfer and recycling at convergent margins: mass–balance and insights from high-P/T metamorphic rocks. In: Bebout, G.E., Scholl, D.W., Kirby, S.H., Platt, J.P. (Eds.), Subduction Top to Bottom. American Geophysical Union, Geophysical Monograph, pp. 179–193.
Belousov, A., Belousova, M., Chen, C.-H., Zellmer, G.F., 2010. Deposits, character and timing of recent eruptions and gravitational collapses in Tatun Volcanic Group, Northern Taiwan: hazard-related issues. J. Volcanol. Geotherm. Res. 191 (3-4), 205–221.
Bottinga, Y., 1969. Calculated fractionation factors for carbon and hydrogen isotope exchange in the system calcite-CO2-graphite–methane–hydrogen and water vapour. Geochim. Cosmochim. Acta 33, 49–64.
Chen, C.-H., Lin, S.B., 2002. Eruptions younger than 20 Ka of the Tatun Volcano Group as viewed from the sediments of the Sungshan Formation in Taipei Basin. West. Pac. Earth Sci. 2, 191–204.
Chen, W.f., Sung, M., 2009. The redox potential of hot springs in Taiwan. Terr. Atmos. Ocean. Sci. 20 (3), 465–479.
Chen, C.H., Wu, Y.T., 1971. Volcanic geology of the Tatun geothermal area, northern Taiwan. Proc. Geol. Soc. China 14, 5–20.
Chen, C., Burr, G., Lin, S., 2010. Time of a Near Holocene volcanic eruption in the Tatun Volcano Group, Northern Taiwan: evidence from AMS radiocarbon dating of charcoalm ash from sediments of the Sungshan formation in Taipei Basin. Terr. Atmos. Ocean. Sci. 21, 611–614.
Clift, P.D., Vannucchi, P., 2004. Controls on tectonic accretion versus erosion in subduction zones: implications for the origin and recycling of the continental crust. Rev. Geophys. Space Phys. 42 (RG2001).
Craig, H., Lupton, J.E., Horibe, Y., 1978. A mantle helium component in Circum-Pacific volcanic gases: Hakone, the Marianas, and Mr. Lassen. In: Alexander, Ozima, M. (Eds.), Terrestrial Rare GasesE.C. Advances in Earth and Planetary Science. Academic Publication, Japan, pp. 3–16.
Fischer, T.P., et al., 2002. Subduction and recycling of nitrogen along the Central American margin. Science 297, 1154–1157.
Fourre, E., Le Guern, F., Jean-Baptiste, P., 2002. Helium isotopes at Satsuma-Iwojima volcano, Japan. Geochem. J. 36, 493–502.
Giggenbach, W.F., Poreda, R.J., 1993a. Helium isotopic and chemical composition of gases from volcanic-hydrothermal systems in the Philippines. Geothermics 22 (5-6), 369–380.
Giggenbach, W.F., Poreda, R.J., 1993b. Helium isotopic and chemical composition of gases from volcanic-hydrothermal systems in the Philippines. Geothermics 22, 369–380.
Haendel, D., Muhle, K., Nitzsche, H.-M., Stiehl, G., Wand, U., 1986. Isotopic variations of the fixed nitrogen in metamorphic rocks. Geochim. Cosmochim. Acta 50 (5), 749–758.
Hilton, D.R., McMurtry, G.M., Goff, F., 1998. Large variations in vent fluid $CO_2/^3He$ ratios signal rapid changes in magma chemistry at Loihi Seamount, Hawaii. Nature 396, 359–362.
Hilton, D.R., Fischer, T.P., Marty, B., 2002. Noble gases and volatile recycling at subduction zones. In: Geochemistry, R.i.M.a. (Ed.)Noble Gases in Geochemistry and Cosmochemistry, pp. 319–370.
Ho, C.S., 1988. An introduction to the geology of Taiwan explanatory text of the geologic map of Taiwan. Central Geological Survey. MOEA (163 pp.).
Hoefs, J., 2009. Stable Isotope Geochemistry (288 pp.).
Ishibashi, J., et al., 1995. Helium and carbon geochemistry of hydrothermal fluids from the Mid-Okinawa Trough Back Arc Basin, southwest of Japan. Chem. Geol. 123 (1–4), 1–15.
Javoy, M., Pineau, F., Iiyama, I., 1978. Experimental determination of the isotopic fractionation between gaseous CO2 and carbon dissolved in tholeiitic magma; a preliminary study. Contrib. Mineral. Petrol. 67, 35–39.
Konstantinou, K.I., Lin, C.H., Liang, W.T., 2007. Seismicity characteristics of a potentially active Quaternary volcano: the Tatun Volcano Group, northern Taiwan. J. Volcanol. Geotherm. Res. 160, 300–318.
Lan, T.F., et al., 2007. Compositions and flux of soil gas in Liu-Huang-Ku hydrothermal area, northern Taiwan. J. Volcanol. Geotherm. Res. 165, 32–45.
Lee, H.-F., et al., 2008. Temporal variations of gas compositions of fumaroles in the Tatun Volcano Group, northern Taiwan. J. Volcanol. Geotherm. Res. 178 (4), 624–635.
Mabry, J., Lan, T., Burnard, P., Marty, B., 2013. High-precision helium isotope measurements in air. Journal of Analytical Atomic Spectrometry 28 (12), 1903–1910.
Marty, B., Jambon, A., Sano, Y., 1989. Helium isotopes and CO_2 in volcanic gases of Japan. Chem. Geol. 76 (1-2), 25–40.
Morris, J.D., Leeman, W.P., Tera, F., 1990. The subducted component in island arc lavas: constraints from Be isotopes and B–Be systematics. Nat. Biotechnol. 344, 31–36.
Ohba, T., et al., 2010. Magmatic fluids of Tatun volcanic group, Taiwan. Appl. Geochem. 25, 513–523.
Poreda, R., Craig, H., 1989. Helium isotope ratios in circum-Pacific volcanic arcs. Nature 338 (6215), 473–478.
Ray, M.C., Hilton, D.R., Munoz, J., Fischer, T.P., Shaw, A.M., 2009. The effects of volatile recycling, degassing and crustal contamination on the helium and carbon geochemistry of hydrothermal fluids from the Southern Volcanic Zone of Chile. Chem. Geol. 266 (1–2), 38–49.
Sadofsky, S.J., Bebout, G.E., 2000. Ammonium partitioning and nitrogen-isotope fractionation among coexisting micas during high-temperature fluid-rock interactions: examples from the New England Appalachians. Geochim. Cosmochim. Acta 64 (16), 2835–2849.
Sano, Y., Marty, B., 1995. Origin of carbon in fumarolic gas from island arcs. Chem. Geol. 119 (1-4), 265–274.
Sano, Y., Wakita, H., 1988. Helium isotope ratio and heat discharge rate in the Hokkaido Island, Northeast Japan. Geochem. J. 22, 293–303.
Sano, Y., Williams, S.N., 1996. Fluxes of mantle and subducted carbon along convergent plate boundaries. Geophys. Res. Lett. 23 (20), 2749–2752.
Sano, Y., Nishio, Y., Sasaki, S., Gamo, T., Nagao, K., 1998. Helium and carbon isotope systematics at Ontake volcano, Japan. Journal of geophysical research 103 (B10), 23863–23873.
Sano, Y., Takahata, N., Nishio, Y., Fischer, T.P., Williams, S.N., 2001. Volcanic flux of nitrogen from the Earth. Chem. Geol. 171 (3-4), 263–271.
Sano, Y., Takahata, N., Seno, T., 2006. Geographical Distribution of 3He/4He Ratios in the Chugoku District. Southwestern Japan. Pure Appl. Geophys. 163, 745–757.
Sano, Y., Tokutake, T., Takahata, N., 2008. Accurate measurement of atmospheric helium isotopes. Anal. Sci. 24 (4), 521–525.
Snyder, G., Poreda, R., Hunt, A., Fehn, U., 2001. Regional variations in volatile composition: isotopic evidence for carbonate recycling in the Central American volcanic arc. Geochem. Geophys. Geosyst. 2.
Snyder, G., Poreda, R., Fehn, U., Hunt, A., 2003. Sources of nitrogen and methane in Central American geothermal settings: noble gas and 129I evidence for crustal and magmatic volatile components. Geochem. Geophys. Geosyst. 4 (1), 9001.
Song, S.R., Tsao, S.J., Lo, H.J., 2000. Characteristics of the Tatun volcanic eruptions, north Taiwan: implications for a cauldron formation and volcanic evolution. J. Geol. Soc. China 43, 361–378.
Takahata, N., Nishio, Y., Yoshida, N., Sano, Y., 1998. Precise isotopic measurements of nitrogen at the sub-nanomole level. Anal. Sci. 14, 485–491.
Ujiie, H., Ujiie, Y., 1999. Late Quaternary course changes of the Kuroshio Current in the Ryukyu Arc region, northwestern Pacific Ocean. Mar. Micropaleontol. 37, 23–40.
Vogel, J.C., Grootes, P.M., Mook, W.G., 1970. Isotopic fractionation between gaseous and dissolved carbon dioxide. Z. Phys. 230, 255–258.
Wang, K.L., et al., 1999. Post-collisional magmatism around northern Taiwan and its relation with opening of the Okinawa Trough. Tectonophysics 308, 363–376.
Wen, S., Chang, Y.-Z., Chen, C.-H., Chen, Y.-G., Teng, T.-L., 2012. The seismic velocity and attenuation structure beneath the Tatun volcanic area, Taiwan. J. Asian Earth Sci. 54–55 (0), 182–191.
Yang, T.F., 2000. $^3He/^4He$ ratios of fumaroles and bubbling gases of hot springs in Tatun Volcano Group, North Taiwan. J. Natl Park 10 (1), 73–94 (in Chinese).
Yang, T.F., Sano, Y., Song, S.R., 1999. $^3He/^4He$ ratios of fumaroles and bubbling gases of hot springs in Tatun Volcano Group, North Taiwan. Nuovo Cimento Soc. Ital. Fis. C 22 (3-4), 281–286.
Yang, T.F., et al., 2003. Sources of fumarolic gases from Tatun Volcano Group, North Taiwan. J. Natl Park 13, 127–156 (in Chinese).
Yang, T.F., Lan, T.F., Lee, H.F., Fu, C.C., Chuang, P.C., Lo, C.H., Chen, C.-H., Chen, C.T.A., Lee, C.S., 2005. Gas compositions and helium isotopic ratios of fluid samples around Kueishantao, NE offshore Taiwan and its tectonic implications. Geochem. J. 39, 469–480.